# $^{123}$I-IODO-BROMSULPHALEIN AS A LIVER AND BILIARY SCANNING AGENT

Michael L. Goris

*Donner Laboratory, University of California, Berkeley, California*

***Bromsulphalein can easily be labeled with $^{123}$I. The potential of this tracer, compared with $^{131}$I-rose bengal and $^{99m}$Tc-labeled colloids, is discussed with reference to experiments on mice and dogs.***

To a large extent $^{99m}$Tc has replaced $^{131}$I for imaging in nuclear medicine. This is well explained by the physical compatibility between the Anger camera and the isotope, even when physiological excellence is lacking. Specifically for the liver, this may have been a loss since not all the information physicians may seek is to be found in the spatial distribution of the reticular cells in the liver. A $^{99m}$Tc-labeled parenchymatous cell tracer has not been developed yet.

Of the tracers processed by the functioning parenchymal cell, rose bengal labeled with $^{131}$I ($^{131}$I-RB) has been used most frequently. The kinetics are not simple (*1*), but there is ample evidence that parenchymal cell tracers can provide information unavailable from data obtained with labeled colloid. The $^{131}$I-RB does allow the differentiation between surgical and nonsurgical jaundice (*2–4*). In infants especially, the patency determination of the biliary pathways by nonaggressive means may be beneficial (*5*) and has led to successful interventions in congenital defects (*6*). The specificity of the tracer for the liver cell has helped in the diagnosis of functional hepatomas (*7*).

Plasma retention curves for $^{131}$I-RB have been used but are not disease-specific (*8*). Sensitivity and specificity differences with Bromsulphalein (BSP) have been found to be due to the measuring techniques or the dose injected (*2,9*).

Iodine-131-labeled tracers fall short when high-resolution, high-quality images are expected with the gamma camera. The reasons are the restriction put on the dose of activity, the relatively low detection efficiency, and the collimation difficulties. For years, W. Myers (*10*) has pleaded the case of $^{123}$I, which decays by electron capture with a 13-hr half-life and has 159-keV photons with 85% abundance. While its physical characteristics compare favorably with those of $^{99m}$Tc, it possesses the labeling characteristics of all iodine isotopes. The labeling technique must be rapid, however, because of the short half-life, and it must have a high yield because of the current high cost of production of $^{123}$I (about $45/mCi). Comparatively, the labeling of rose bengal is more time consuming (*11*) than the convenient method described by Suwanik and Tubis (*12*) for BSP. In this work, we hope to demonstrate how $^{123}$I-BSP potentially combines the advantages of $^{131}$I-RB and $^{99m}$Tc-colloid in liver function and morphology evaluation.

## MATERIALS AND METHODS

**Labeling.** The Suwanik and Tubis method (*12*) was used with only slight modifications. In short, to a mixture of radioiodide, with no carrier added, of the desired activity, 0.1 cc of KI (2 mg/ml) and 0.1 cc of $KIO_3$ (2 mg/ml), one adds 0.3 cc of 1 *N* HCl followed by 1 cc of BSP (Bromsulphalein®, Hyson, Westcott and Dunning, Inc.) (50 mg/ml). Subsequently, the pH is brought to 3 with HCl, and the mixture is shaken and allowed to stand at room temperature for 30 min. At the end of this time, the pH is brought to 6–7 with NaOH and the mixture is collected in a syringe prefilled with 1 cc of AG1-X8 resin (100-200 mesh, chloride form, Bio-Rad Laboratories). For this purpose the resin is pre-equilibrated with normal saline. As the resin sediments, the superfluous saline is removed and 1 cc of the

Received Mar. 30, 1973; revision accepted June 26, 1973.

For reprints contact: Michael L. Goris, Donner Laboratory, University of California, Berkeley, Calif. 94720.

sedimented resin is aspirated in a 5-cc syringe. When the mixture is aspirated into the syringe, not more than 4 cc are filled, and enough air can be introduced to allow adequate mixing by shaking. A disposable Millipore unit (Swinnex®-13, 0.22 μm, Millipore Corporation) is then fitted to the syringe, the resin is allowed to sediment at the filter end of the syringe, and the contents are subsequently injected through the filter into a multidose injection vial. The resin, to which the free iodide is fixed, does not pass through the filter. For the mouse experiments, the label was $^{125}I$ and for the dog experiments $^{123}I$. In all cases, the specific activity was at least 40 μCi/mg BSP.

**Testing.** The labeled tracer, $^{125}I$-BSP, was injected intravenously into male Swiss mice weighing between 27 and 34 gm. Blood samples were taken over an interval of 15 min. In one series, a mixture of $^{125}I$-BSP and $^{131}I$-RB (Robengatope®, E. R. Squibb and Sons) was injected for simultaneous analysis and comparison of the kinetics of those tracers. The total amount of BSP and its iodinated derivative, $^{125}I$-BSP, injected was approximately 0.2 mg (7 mg/kg). The data were analyzed for comparison according to a two-compartment model (Fig. 1). The shelf stability of the compound was documented by Suwanik and Tubis (*12*). In vivo stability was tested by comparing the thyroidal uptake (as fraction of the injected dose) 1 hr after injection, to the thyroidal uptake of $Na^{131}I$ in mice who were kept on an iodine-free diet for 8 days. From those experiments it was estimated that not more than 1% of the injected activity was free iodide during the course of the experiments. Iodine-123-BSP was injected intravenously in Beagle dogs (10 kg, either sex), and the distribution of the tracer followed with an Anger camera. The activity ranged from 0.15 to 1.5 mCi and the total amount of BSP and $^{123}I$-BSP from 4 to 40 mg (0.4 to 4 mg/kg). In one case, the dog had been previously injected with a $^{99m}Tc$-S-colloid (Tesuloid®, E. R. Squibb and Sons) and the two studies were compared. With the camera, the spectral separation was possible only by using the upper half of $^{123}I$ 159-keV photopeak. This reduced the counting rate from the previously administered technetium tracer by a factor of five.

In every case, a parallel-hole (low-energy) collimator was used until most of the activity was localized in the gallbladder. Subsequently, pictures of the gallbladder were taken with the pinhole collimator.

The camera was interfaced with a computer, as described by Budinger (*13*). Data were accumulated in histogram mode with frames of 15 sec. Each study required at least 1 hr for completion while a high

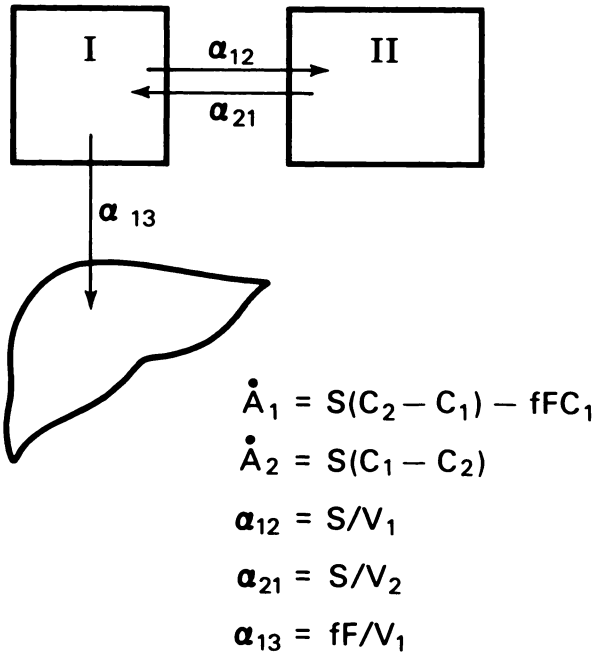


**FIG. 1.** Two-compartmental model for bromsulphalein and rose bengal. Analysis of rate of change $A_1$ of quantity of tracer present in compartment i is based on following assumptions: (a) Tracer is restricted to Compartments I and II, between which there is exchange, and third compartment, liver, which acts as sink. (b) In each compartment there is instantaneous mixing. (c) Kinetics are first order at all times. (d) System is defined by following constant values:

$V_i$ is volume of compartment i
f is extraction efficiency by liver
F is blood flow to liver
S is average permeability multiplied by area of interface between compartments I and II

Rate of change $A_1$ is due to differences in concentration between Compartment I and Compartment II ($C_2 - C_1$) multiplied by S, and rate of liver uptake, $fFC_1$. Rate of change $A_2$ is exclusively due to concentration differences ($C_1 - C_2$), multiplied by S. Fractional turnover rates $\alpha_{ij}$ are defined as shown and represent fraction of tracer present in compartment i going to compartment j per unit of time. If Q is amount initially introduced in Compartment I, solutions to the set of differential equations are $A_1(t) = Q(I_1e^{-s_1t} + I_2e^{-s_2t})$ and $A_2(t) = QI_3(e^{-s_2t} - e^{-s_1t})$. In terms of fractional turnover rates $\alpha_{ij}$, we have: $I_1 + I_2 = 1$; $I_1s_2 + I_2s_1 = \alpha_{21}$; $s_1 + s_2 = \alpha_{12} + \alpha_{13} + \alpha_{21}$; $s_1s_2 = \alpha_{12}\alpha_{21}$; $I_2(s_1 - s_2) = \alpha_{12}$.

counting rate was needed for the quality of the static images with which the Tc-colloid images were compared.

A square area circumscribed by the detector circumference was mapped into a 64 × 64 matrix. Polaroid pictures for the morphological evaluation were generated directly from the camera's CRT display while the data accumulated by the computer were used for the generation of time functions from rectangular regions of interest and for teletype display in one of the following modes: (A) the original data, collected in 15-sec frames divided into 4,096 matrix elements (64 × 64), are recombined by addition into frames of 1 min (or longer, depending on the counting rate) in any given experiment. Furthermore, this new frame is reduced to a 1,024

**TABLE 1. FITTING PARAMETERS AND DERIVED PHYSIOLOGICAL VALUES FROM PLASMA DISAPPEARANCE CURVES IN MICE**

| | $^{125}$I-BSP | | | | | | | | | |
|---|---|---|---|---|---|---|---|---|---|---|
| Mouse No. | 1 | 2 | 3 | 4 | 7 | 11 | 12 | 13 | 14 | 15 |
| $I_1$ | 0.985 | 0.975 | 0.983 | 0.984 | 0.973 | 0.961 | 0.948 | 0.967 | 0.963 | 0.942 |
| $I_2$ | 0.015 | 0.025 | 0.017 | 0.016 | 0.027 | 0.039 | 0.052 | 0.033 | 0.037 | 0.058 |
| $T_2$(min) | 9.40 | 8.80 | 12.4 | 15.0 | 15.0 | 9.50 | 9.00 | 10.5 | 18.0 | 11.2 |
| $T_1$(min) | 0.65 | 0.60 | 0.55 | 0.58 | 0.45 | 0.80 | 1.10 | 0.70 | 0.90 | 1.10 |
| $s_2$(min$^{-1}$) | 0.074 | 0.079 | 0.056 | 0.046 | 0.046 | 0.073 | 0.077 | 0.066 | 0.038 | 0.062 |
| $s_1$(min$^{-1}$) | 1.066 | 1.155 | 1.260 | 1.195 | 1.540 | 0.866 | 0.630 | 0.990 | 0.770 | 0.900 |
| $V_1$(ml) | 2.385 | 1.752 | 1.534 | 2.817 | 1.393 | 2.624 | 1.833 | 2.532 | 3.026 | 2.887 |
| 12 | 0.162 | 0.263 | 0.313 | 0.302 | 0.664 | 0.223 | 0.140 | 0.278 | 0.287 | 0.346 |
| 21 | 0.088 | 0.105 | 0.076 | 0.063 | 0.085 | 0.103 | 0.105 | 0.096 | 0.065 | 0.110 |
| 13 | 0.889 | 0.866 | 0.927 | 0.876 | 0.837 | 0.613 | 0.462 | 0.682 | 0.457 | 0.506 |
| fFml/min | 2.12 | 1.55 | 1.42 | 2.47 | 1.16 | 1.61 | 0.85 | 1.73 | 1.38 | 1.46 |
| $V_2$ml | 4.38 | 4.38 | 6.32 | 39.2 | 10.9 | 5.67 | 2.44 | 7.35 | 13.4 | 9.07 |

In the mouse experiments, the observations are activity per volume as a function of time in the intravascular Compartment I. The data could be fitted by the function $In_1e^{-s1t} + In_2e^{-s2t}$. The correspondence with solutions presented in Fig. 1 is found as follows:

$$Q/(In_1 + In_2) = V_1;\ In_1/Q = I_1;\ In_2/Q = I_2;\ \alpha_{21} = I_1s_2 + I_2s_1;\ \alpha_{12} = s_1s_2/\alpha_{21};$$
$$\alpha_{12} = s_1 + s_2 - \alpha_{13} - \alpha_{21};\ fF = \alpha_{12}V_1;\ V_2 = \alpha_{12}V_1/\alpha_{21}.$$

$T_1$ and $T_2$ are the half-lives corresponding to $s_1$ and $s_2$. From this computation procedure, it follows that the effect of error propagation will be very large for $V_2$, and larger for fF and $\alpha_{12}$ than for $\alpha_{21}$ and $\alpha_{13}$. This is reflected in the wide variation of the parameters from different mice. The values are printed beyond their last significant digit to allow the reader to check the computation without undue rounding errors.

**TABLE 2. $^{131}$I-RB, DONE SIMULTANEOUSLY WITH BSP IN MICE NO. 11–15 IN TABLE 1**

| Mouse No. | 11 | 12 | 13 | 14 | 15 |
|---|---|---|---|---|---|
| $I_1$ | 0.892 | 0.981 | 0.869 | 0.889 | 0.797 |
| $I_2$ | 0.108 | 0.119 | 0.131 | 0.111 | 0.203 |
| $T_2$(min) | 15.0 | 9.00 | 10.5 | 17.5 | 10.2 |
| $T_1$(min) | 1.10 | 1.50 | 1.15 | 1.35 | 1.60 |
| $s_2$(min$^{-1}$) | 0.046 | 0.077 | 0.066 | 0.040 | 0.068 |
| $s_1$(min$^{-1}$) | 0.630 | 0.462 | 0.603 | 0.513 | 0.433 |
| $V_1$(ml) | 2.070 | 2.108 | 2.520 | 2.456 | 2.499 |
| 12 | 0.300 | 0.032 | 0.240 | 0.238 | 0.152 |
| 21 | 0.108 | 0.084 | 0.136 | 0.098 | 0.141 |
| 13 | 0.268 | 0.423 | 0.293 | 0.223 | 0.209 |
| fFml/min | 0.55 | 0.89 | 0.74 | 0.55 | 0.52 |
| $V_2$ml | 5.75 | 0.80 | 4.45 | 6.35 | 2.68 |

The compuation is the same as in Table 1. The data were collected after a simultaneous injection of $^{125}$I-BSP and $^{131}$I-RB in Mice 11–15, and the results should be compared with those of corresponding mice in Table 1.

matrix (32 × 32) by replacing four original matrix elements (in a two-by-two array) with one containing the average value. The reduced frame is printed out, coded from 10 (for the maximum value within the frame) to 0, in a linear fashion. (B) The reduction to 32 × 32 frame was not performed, and a region of the frame was printed out in a logarithmic code where 10 = 100%, 5 = 10%, 0 = 1% of a preset value, a type of display allowing for the evaluation of spatial distribution changes in time over a larger range of values with two-digit symbols although with smaller sensitivity than in linear scales.

## RESULTS AND DISCUSSION

**Experiments in mice.** The results for $^{125}$I-BSP are summarized in Table 1 and for $^{131}$I-RB in Table 2. Using the compartmental assumptions of Fig. 1, one can compute from Q, the injected dose, and from $In_1$, $In_2$, the intercepts, and $s_1$, $s_2$, the slopes, the following physiological values: $\alpha_{12}$ (min$^{-1}$), the fractional turnover rate from the intra- to the extra-

**TABLE 3. FITTING PARAMETERS AND DERIVED PHYSIOLOGICAL VALUES FROM THE POOLED PLASMA DISAPPEARANCE RATE DATA**

| | Group 1 BSP | Group 2 BSP | Group 2 RB |
|---|---|---|---|
| $I_1$ | 0.978 | 0.954 | 0.850 |
| $I_2$ | 0.022 | 0.046 | 0.150 |
| $T_2$ | 10 min | 9.5 min | 10.3 min |
| $T_1$ | 0.65 min | 0.9 min | 1.3 min |
| $s_2$ | 0.069 min$^{-1}$ | 0.073 min$^{-1}$ | 0.067 min$^{-1}$ |
| $s_1$ | 1.066 min$^{-1}$ | 0.77 min$^{-1}$ | 0.533 min$^{-1}$ |
| $V_1$ | 2.0 | 2.5 | 2.3 |
| 12 | 0.228 | 0.208 | 0.202 |
| 21 | 0.090 | 0.105 | 0.137 |
| 13 | 0.817 | 0.535 | 0.261 |
| fF | 1.634 | 1.337 | 0.600 |
| $V_2$ | 5.1 | 4.8 | 3.4 |

The data are pooled after normalizing in regard to the sum of the intercepts $I_1 + I_2$. The value for $V_1$ is the average of the values found for corresponding mice and tracers in Tables 1 and 2. Group 1 is composed of Mice 1–7 and Group 2 of Mice 11–15, on which the simultaneous determinations for $^{125}$I-BSP and $^{131}$I-RB were performed. Since the determinations were simultaneous for both tracers in Group 2, the difference between fF for $^{125}$I-BSP and $^{131}$I-RB is due to a larger extraction efficiency for the former.

**TABLE 4. DISTRIBUTION OF THE TOTAL DOSE BETWEEN LIVER AND NONLIVER COMPARTMENTS (BLOOD+TISSUES) AT EARLY TIMES**

| | BSP | | | RB | | |
|---|---|---|---|---|---|---|
| Time (min) | Blood + Tissue | Liver | Ratio | Blood + Tissue | Liver | Ratio |
| 0.0 | 1.0 | 0.0 | 0.0 | 1.0 | 0.0 | 0.0 |
| 0.5 | 0.777 | 0.223 | 0.287 | 0.883 | 0.117 | 0.132 |
| 1.0 | 0.620 | 0.380 | 0.612 | 0.790 | 0.210 | 0.265 |
| 2.0 | 0.433 | 0.567 | 1.309 | 0.655 | 0.345 | 0.526 |
| 5.0 | 0.247 | 0.753 | 3.040 | 0.446 | 0.554 | 1.242 |
| 10.0 | 0.162 | 0.838 | 5.172 | 0.298 | 0.702 | 2.355 |

In the mouse experiments, the intravascular compartment was the only one sampled, but the derivations shown under Table 1 allowed us to derive all the parameters defined in the model in Fig. 1. In this way, to the extent that the assumptions are valid, the kinetics of both tracers are completely defined. The activity in blood and tissue is the sum of the activity in Compartments I and II and is equal to:

$$Q(I_1 - I_3)e^{-s_1 t} + (I_3 + I_2)e^{-s_2 t})$$

The activity of liver is equal to:

$$\alpha_{12} Q \int_0^t (I_1 e^{-s_1 t} + I_2 e^{-s_2 t})dt.$$

Using the values found for Group 2 in Table 3 and the fact that $I_3 = \alpha_{12}/(s_1 - s_2)$, while assuming that the injected amount is unity, allowed us to compute the expected values for intra- and extrahepatic activity. The ratio hepatic/extrahepatic is an estimate of the target-to-background ratio assuming equal volume distributions.

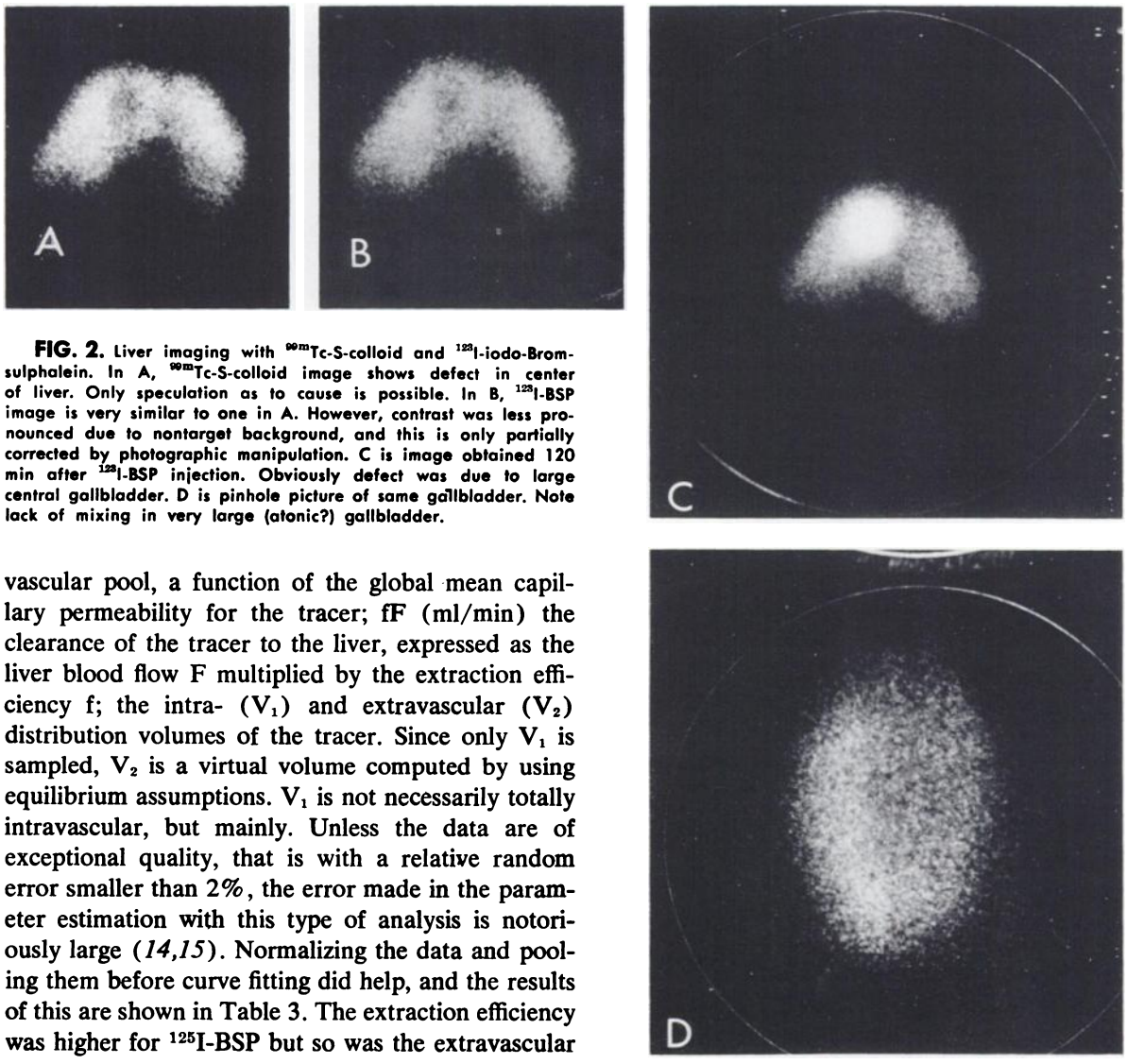


**FIG. 2.** Liver imaging with $^{99m}$Tc-S-colloid and $^{123}$I-iodo-Bromsulphalein. In A, $^{99m}$Tc-S-colloid image shows defect in center of liver. Only speculation as to cause is possible. In B, $^{123}$I-BSP image is very similar to one in A. However, contrast was less pronounced due to nontarget background, and this is only partially corrected by photographic manipulation. C is image obtained 120 min after $^{123}$I-BSP injection. Obviously defect was due to large central gallbladder. D is pinhole picture of same gallbladder. Note lack of mixing in very large (atonic?) gallbladder.

vascular pool, a function of the global mean capillary permeability for the tracer; fF (ml/min) the clearance of the tracer to the liver, expressed as the liver blood flow F multiplied by the extraction efficiency f; the intra- ($V_1$) and extravascular ($V_2$) distribution volumes of the tracer. Since only $V_1$ is sampled, $V_2$ is a virtual volume computed by using equilibrium assumptions. $V_1$ is not necessarily totally intravascular, but mainly. Unless the data are of exceptional quality, that is with a relative random error smaller than 2%, the error made in the parameter estimation with this type of analysis is notoriously large (*14,15*). Normalizing the data and pooling them before curve fitting did help, and the results of this are shown in Table 3. The extraction efficiency was higher for $^{125}$I-BSP but so was the extravascular

volume ($V_2$). Early, the computed fraction taken up by the liver was larger for BSP. Table 4 illustrates the early ratio between liver and nonliver activity (Compartment 1 and 2). At later times, redistribution within the liver would prevent comparison with $^{99m}$Tc-colloid scans. From the mice experiments, therefore, a significant improvement over $^{131}$I-RB was expected beyond those due to the physical characteristics of $^{123}$I.

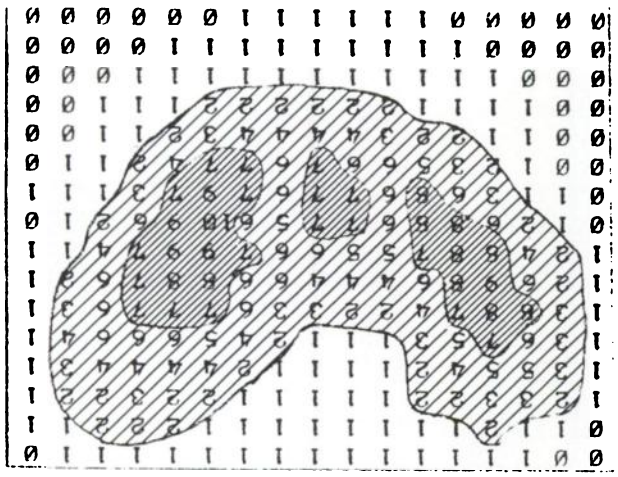


**FIG. 3.** Teletype printout of $^{123}$BSP liver image. Liver is same as shown in Fig. 2. Data were originally collected in 64 × 64 matrix with integration time of 15 sec. From this, frames of 60 sec are generated by additions, and those are reduced to 32 × 32 frames by adding matrix elements (four matrix elements in two-by-two array), to print frame on teletype with two-digit symbols with minimal distortion. In this case, 10 stands for 1,492 counts, and scale is linear.

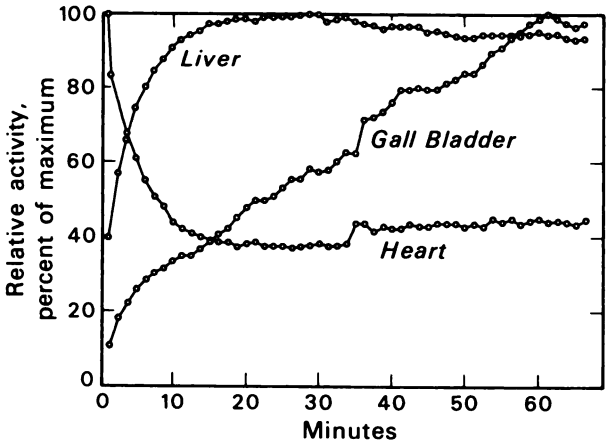


**FIG. 4.** Time functions of regional activity over heart, liver, and gallbladder. Time functions are uncorrected for cross-talk, that is, influence of scattered rays originating in one region, on time function of another region. Liver time function includes gallbladder time function. One has to remember that in external detection, sampling is never pure and each curve represents linear combination of activities originating in different subsystems. Hence, heart curve is mostly due to intra- and extravascular activity (Compartments I and II from Fig. 1) but, due to overlapping in projection surface, may be influenced by liver and gallbladder activity. Liver curve contains large element due to intra- and extravascular, but extrahepatic activity. Due to small change in position of dog, between 30 and 40 min artifact is more visible on heart and gallbladder curves which were generated from smaller regions of interest than liver one.

**External detection in Beagle experiments.** In Figs. 2A and B, liver images are shown with $^{99m}$Tc-S-colloid and $^{123}$I-BSP, respectively, that were performed sequentially on the same dog. Initially, the resolution was similar, as expected, even considering the lower target-to-nontarget ratio for $^{123}$I-BSP at that time (10 min postinjection). A relatively high nonliver background was still present, as shown in Fig. 3 (a printout of the reduced 32 × 32 matrix) at 19 min postinjection. At 120 min most of the activity was in the gallbladder (Fig. 2C), also shown with a pinhole picture (Fig. 2D).

Time curves for heart, liver, and gallbladder are shown in Fig. 4.

Disappointingly, the nonliver activity (heart) did not reach values much lower than 50% of its initial value. A part of this may be explained by the increasing interference of scattered rays originated from higher energy radiation from an $^{130}$I contaminant as increasing amounts of the tracer concentrated in the field of the camera. Thirteen minutes after injection, the departure of the gallbladder curve from the characteristics of the liver curve reflects gallbladder accumulation. This is also illustrated in Fig. 5 showing the time-distribution relation of the tracer in a logarithmic display. Since the dog gallbladder, unlike that of man, is located in the center of the liver, its activity interfered more with the demonstration of the liver clearance that would be expected in humans. An interesting view of the gallbladder is shown in Fig. 6.

Inasmuch as $^{123}$I-BSP does indeed behave in a manner similar to $^{131}$I-RB, it will furnish the same type of information otherwise not available from colloidal scanning agents. Since the isotope can be given in higher doses and is compatible with the Anger camera, pictorial information approaching the quality expected of $^{99m}$Tc agents can be gained. The restriction lies in the relatively high nontarget background and the interference of the contaminant. On the other hand, $^{123}$I-BSP is shown to provide images of very high quality of the gallbladder.

ACKNOWLEDGMENT

This work was supported in part by the USAEC under the contract No. W-7405-eng-48, and the Bay Area Heart Research Association, and the NFWO (Belgian National Foundation for Scientific Investigation).

REFERENCES

1. LUSHBAUGH CC, KRETCHMAR A, GIBBS W: Liver function measured by the blood clearance of rose bengal-

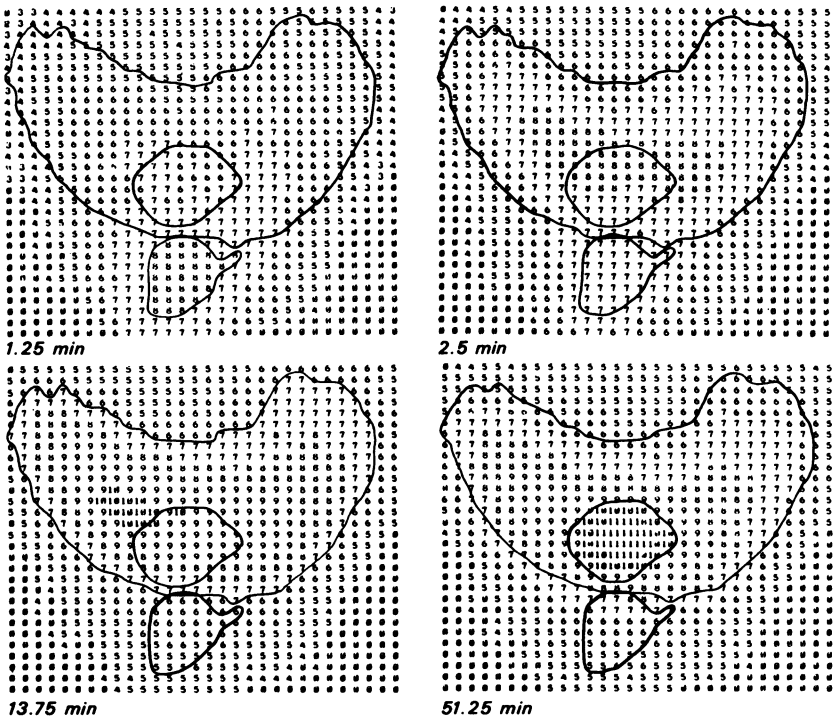


**FIG. 5.** Image of gallbladder obtained with $^{123}$I-BSP. Pinhole was directed in ventrocaudal to craniodorsal direction and positioned in contact with abdominal wall of dog.

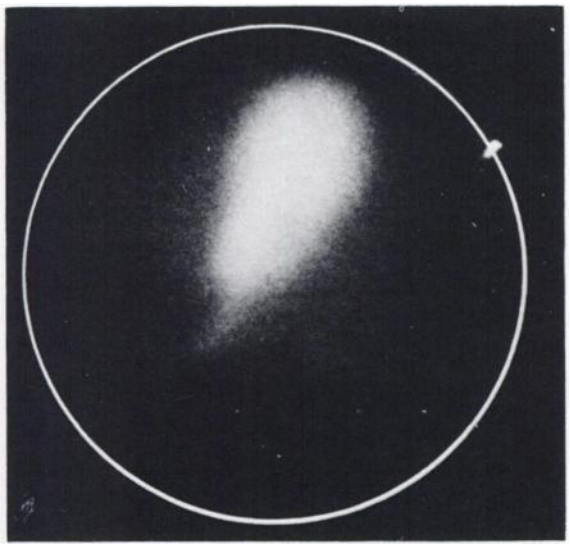

**FIG. 6.** Time-distribution of $^{123}$I-BSP in dog. In display, frames represent counts integrated over 1 min, as in Fig. 3. However, reduction to 32 × 32 matrix was not performed. Code is logarithmic, in four frames, 10 = 873 counts, 5 = 87, and 0 = 8. Heart, liver, and gallbladder regions are delineated to emphasize distribution changes.

$^{131}$I: a review and a model based on compartmental analysis of changes in arm, blood, and liver radioactivity. In *Dynamic Clinical Studies with Radioisotopes*, Kniseley RM, Tauxe WM, Anderson EB, eds, CONF 355, TID 7678, Oak Ridge, Tenn, USAEC, 1964, pp 319–357

2. NORDYKE RA: Surgical vs. non-surgical jaundice. Differentiation by a combination of rose bengal-$^{131}$I and standard liver-function tests. *JAMA* 194: 949–953, 1965

3. EYLER WR, SCHUMAN BM, DU SAULT LA: The radioiodinated rose bengal liver scan as an aid in the differential diagnosis of jaundice. *Am J Roentgenol* 94: 469–476, 1965

4. CLARK JS, BARRET P, FONKALSRUD ED, et al: Diagnosis of obstructive jaundice. *Calif Med* 112: 44–58, 1970

5. SHARP HL, KRIVIT W, LOWMAN JT: The diagnosis of complete intrahepatic obstruction by rose bengal-$^{131}$I. *J Pediatr* 70: 46–53, 1967

6. WILLIAMS LE, FISHER JH, COURTNEY RA: Preoperative diagnosis of choledochal cyst by hepatoscintigraphy. *N Engl J Med* 283: 85–86, 1970

7. SHOOP JD: Functional hepatoma demonstrated with rose bengal scanning. *Am J Roentgenol* 107: 51–53, 1969

8. ROSENTHALL L: The application of colloidal radiogold and radioiodinated rose bengal in hepatobiliary disease. *Am J Roentgenol* 101: 561–569, 1967

9. UTHGENANNT H, DAHL P, PIENING O: Vergleichende Untersuchungen mit dem Radio-Bengalrosa-und dem Bromsulphalein-Test. *Dtsch Med Wochenschr* 91: 211–216, 1966

10. MYERS WF, ANGER HO: Radioiodine-123. *J Nucl Med* 3: 183, 1962

11. HALLABA E, RAIEH M: Photo-induced labelling of rose bengal with $^{131}$I by ultra-violet radiation. *Int J Appl Radiat Isot* 18: 533–535, 1967

12. SUWANIK R, TUBIS M: A simplified method for the preparation of $^{131}$I-labelled sulfobromophtalein. *Int J Appl Radiat Isot* 19: 883, 1968

13. BUDDINGER TF: Clinical and research quantitative nuclear medicine system. In *Medical Radioisotopes Scintigraphy*. Vienna, IAEA, 1973

14. MYHILL J, WADSWORTH GP, BROWNELL GL: Investigation of an operator method in the analysis of biological tracer data. *Biophys J* 5: 89–107, 1965

15. MYHILL J: Investigation of the effect of data error in the analysis of biological tracer data. *Biophys J* 7: 903–911, 1967